IEEE Photonics Journal
An IEEE Photonics Society Publication

Open Access

Ultrafast and Broadband Terahertz Modulator With Polarization Selectivity

Volume 11, Number 6, December 2019

Hongchuan He
Qiuping Huang
Honglei Cai
Yi Zhao
Xiaoxia Lin
Hao Cheng
Tian Ma
Jianlin Wang
Haoliang Huang
Ming Yin
Zhengping Fu
Yalin Lu

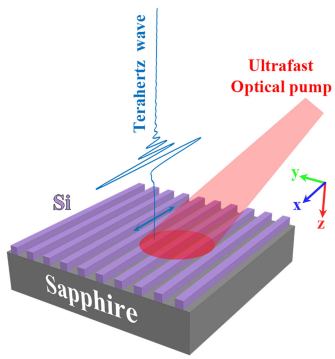

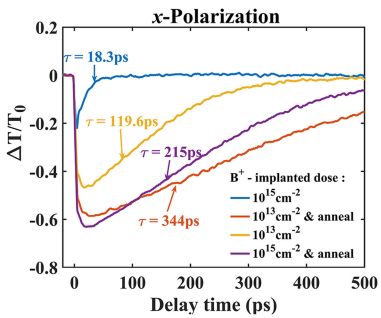

DOI: 10.1109/JPHOT.2019.2947993

Ultrafast and Broadband Terahertz Modulator With Polarization Selectivity

Hongchuan He,[1] Qiuping Huang,[2,4] Honglei Cai,[2] Yi Zhao,[2] Xiaoxia Lin,[2] Hao Cheng,[1] Tian Ma,[3] Jianlin Wang,[3] Haoliang Huang,[3] Ming Yin,[3] Zhengping Fu,[1,2,3] and Yalin Lu[1,2,3,4]

[1]Department of Materials Science and Engineering, University of Science and Technology of China, Hefei 230026, China
[2]Hefei National Laboratory for Physical Sciences at the Microscale, University of Science and Technology of China, Hefei 230026, China
[3]Anhui Laboratory of Advanced Photon Science and Technology, National Synchrotron Radiation Laboratory, University of Science and Technology of China, Hefei 230026, China
[4]Quantum Materials and Photonic Technology Laboratory, Synergetic Innovation Center of Quantum Information and Quantum Physics, University of Science and Technology of China, Hefei 230026, China

DOI:10.1109/JPHOT.2019.2947993

Manuscript received September 18, 2019; accepted October 15, 2019. Date of publication October 28, 2019; date of current version November 20, 2019. This work was supported in part by the National Natural Science Foundation of China under Grants 11704373 and 51627901, in part by Chinese Universities Scientific Fund (WK2340000071), and in part by Anhui Initiative in Quantum Information Technologies under Grant AHY100000. Corresponding authors: Qiuping Huang and Yalin Lu (e-mail: qphuang@ustc.edu.cn; yllu@ustc.edu.cn).

Abstract: We demonstrate a broadband and polarization selective terahertz modulator with ultrafast modulation speed, based on the Si grating metasurface on the Sapphire substrate. The Si layer is implanted with B^+ and subsequently annealed, which significantly reduces the lifetime of carriers and increases the carrier density, and thus realizes ultrafast and efficient modulation. Our modulator achieves modulation depth up to 60% for the *x*-polarized THz wave and less than 1% for the *y*-polarized THz wave in the frequency ranging from 0.5 to 2.5 THz, with switch-on and switch-off time of modulation in 20 ps and around 300 ps, respectively. The carrier dynamics of the fabricated Si grating is also studied to illustrate the ultrafast modulated mechanism. Our results pave the way for ultrafast manipulation of terahertz spectrum and shows great potential in terahertz communication.

Index Terms: Terahertz (THz) spectrum, modulator, ultrafast.

1. Introduction

In recent years, terahertz (THz) technologies have attracted tremendous attention for their promising applications in imaging [1], non-destructive examination [2], high-speed wireless communication [3], THz spectroscopy [4], etc. Hence, efficient THz devices and components are highly desirable to promote the performance of these THz technologies. Among them, THz modulators that can be employed as switchers, light filter, and beam splitters play important roles in many THz systems. For realization of active THz modulators, various types of functional materials or structures have been employed and designed [5]–[13]. Much effort has been devoted to obtaining both broadband modulation and large modulation-depth [8]–[13]. For example, under the photo-excitation of a cw-laser, broadband THz intensity has been highly modulated in the organics/silicon bi-layers [8], graphene on Si [9], and graphene on Ge [10]. With combination of photoexcitation and gate

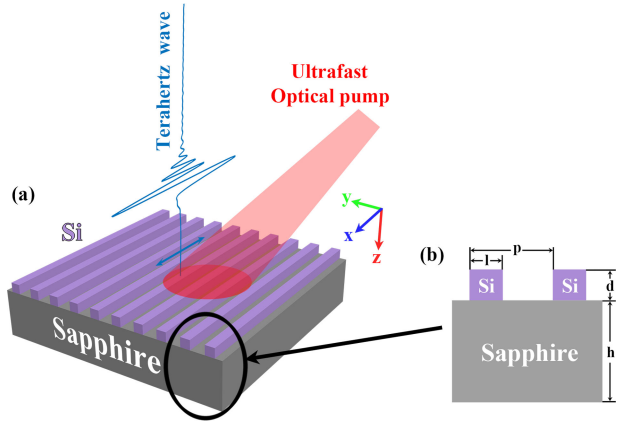

Fig. 1. (a) Schematic illustration of the polarization sensitive SOS-grating metasurface. The *x*-polarized THz wave can be ultrafast optically modulated. (b) Geometry of SOS-grating metasurface. The depth of Si-epilayer is $d = 600$ nm and thickness of Sapphire substrate is $h = 530$ μm. The period of grating p and the filling factor l/p vary in the simulation.

voltage, a larger modulation depth can be achieved in the graphene/Si structure [11]. Other works by applying a gated voltage, large THz modulation has also been demonstrated in the VO_2-intergrated metasurface [12], and in the $BiFeO_3$/Si structure [13]. However, these devices suffered from the low modulation speed. Under some applications, such as THz wireless communication, ultrafast modulation is strongly demanded.

To date, some ultrafast THz modulators have been demonstrated based on the hybrid semiconductor/metasurface or semiconductor plasmonic metasurfaces, like incorporating the organic-inorganic hybrid lead halide perovskites $MAPbI_3$ into the split-ring resonators (SRRs) [14], combining the ErAs/GaAs superlattices [15] or the radiation-damaged Si [16] with the SRRs, utilizing photonic crystal based on GaAs [17], integrating asymmetric SRRs with Ge [18] or MoS_2 [19], and employing Si [20] or GaAs [21] plasmonic structures. Ultrafast switch on of modulation is triggered by photo-doping the under lying semiconductor film or structure using a femtosecond laser pulse. And the switch-off time of modulation is dependent on the fast carrier recombination time of semiconductors. However, in these devices, modulation has been accomplished by utilizing resonances of the SRRs or plasmonic resonances, so such modulation presents a narrow operation band.

In this paper, we propose a grating-like metasurface based on Silicon-On-Sapphire (SOS) substrate which not only realizes the function of ultrafast modulation of broadband terahertz wave, but also shows the ability of polarization selectivity. Due to the intrinsic Si has a long carrier recombination lifetime on the order of milliseconds, ion implanting is a considerable method to reduce the carrier lifetime of Si [22]. Therefore, the SOS in our experiments is implanted with boron ion (B^+) and with/without subsequently annealed to improve the crystalline quality of Si, in order to reduce the carrier lifetime of Si and realize the ultrafast modulation. To investigate the ultrafast modulation response caused by ion-implantation and annealing, four types of SOS gratings were fabricated and measured. The experimental results show we can achieve a broadband modulator working from 0.5 to 2.5 THz by means of optical-pump terahertz-probe spectroscopy with the maximum modulation depth up to 60% for the *x*-polarized THz wave and less than 1% for the *y*-polarized THz wave. And the modulation on and off time is in 20 ps and around 300 ps, respectively. Moreover, the carrier dynamics of the fabricated SOS grating is also studied and analyzed.

2. Design and Simulation Section

The schematic diagram of the polarization sensitive SOS-grating metasurface is depicted in Fig. 1. The Si grating metasurface is designed above the Sapphire substrate with thickness of 530 μm. In order to achieve the effect of ultrafast modulation of broadband terahertz wave with polarization

selectivity, we firstly simulated the transmission spectra of our SOS-grating metasurface by using the Finite Element Method (FEM) with a commercial software COMSOL Multiphysics. The periodical boundary conditions are applied in the *x*- and *y*-directions, whereas Floquent periodic ports are adopted in the *z*-direction. The mesh count of the model geometry is about 50,000 to calculate a reliable simulation results. The period *p* and filling factor *l/p* vary in the simulation. The dielectric constant of sapphire substrate is set to 10.5 [23]. The dielectric function of Si film of SOS can be expressed by the Drude model as [24]:

$$\varepsilon_{Si} = \varepsilon_{\infty} - \frac{{\omega_p}^2}{\omega^2 + i\omega/\tau_d} \tag{1}$$

where ε_{∞} is the high frequency dielectric constant and $\varepsilon_{Si,\infty} = 11.7$, $\tau_d = 80$ fs is the Drude model carrier scattering rate [20], the plasma frequency of Si is expressed as:

$$\omega_p = \sqrt{N e^2/\varepsilon_0 m^*} \tag{2}$$

where e is the electron charge and ε_0 is vacuum permittivity, N is the carrier density, $m^* = (m_e^{*-1} + m_h^{*-1})^{-1} = 0.15 m_e$ (m_e is the electron mass) is the effective mass of the carriers calculated by DFT [25]. In our simulation, the carrier concentration of Si is assumed to vary from 10^{17} cm^{-3} to 10^{19} cm^{-3}.

The simulated transmission spectra of the SOS grating depending on different Si carrier concentration for *x*-polarized and *y*-polarized THz wave are demonstrated in Fig. 2. From Figs. 2(a) and 2(b), it can be seen that the SOS-grating metasurface has an excellent polarization selectivity. The *y*-polarized THz wave is slightly modulated with the variation of Si carrier concentration. However, with the incidence of *x*-polarized wave, our SOS-grating metasurface shows a broadband modulation band, and deep modulation depth up to 57.1% (defined as the variation of electric field transmission, which is calculated as $|T\text{-}T_0|/T_0$, T_0 represents the transmission of the grating without optical modulated while T represents the transmission of the grating under optical modulated) at 1 THz when the carrier concentration of Si increases from 10^{17} cm^{-3} to 10^{19} cm^{-3}. As is shown in Figs. 2(c) and 2(e), the *x*-polarized THz wave are always modulated as the Si carrier concentration changes in different geometry of SOS-metasurface. And the modulation depth slightly decreases with the increasing period, while obviously increases with the increasing filling factor. However, for the *y*-polarized THz wave with results shown in Figs. 2(d) and 2(f), the modulation depth is almost close to zero with the increasing period. Until the period value is larger than 30 μm, the modulation depth begins to increase with the increasing period. On the other hand for the *y*-polarized THz wave, the modulation depth keeps close to zero and doesn't increase with the increasing filling factor until the fill factor becomes larger than 0.5. Therefore, in order to obtain a high modulation depth and also realize the modulation of polarization selectivity, we set the period value and filling factor value in the experiment to be 10 μm and 0.4, respectively.

3. Experimental Results and Discussions

3.1 Sample Fabrication

As the simulation results indicate, we fabricated the grating-like metasurface on the SOS wafers, which consists of a 600 nm-thick Si epitaxial layer on 530 μm-thick and 10 mm $\times$ 10 mm-area A-plane sapphire substrate. The Si epilayer was heavily *p*-doped by boron ion (B^+) implantation and post-processed via rapid thermal annealing (RTA), which improved the carrier density and reduced the carrier lifetime of Si [26]. To investigate the ultrafast modulation response caused by ion implantation and RTA, we fabricated four different types of silicon layer in SOS by B^+ implantation at the dose of 10^{15} cm^{-2} or 10^{13} cm^{-2} at 100 keV, and were post-processed with or without annealed at 1000 °C via RTA. Then four SOS-grating samples were fabricated by UV-photolithographically protection and subsequent reactive ion etching (RIE). As is shown in Fig. 2(e), the period of each SOS-grating is 10 μm and the filling factor is 0.4.

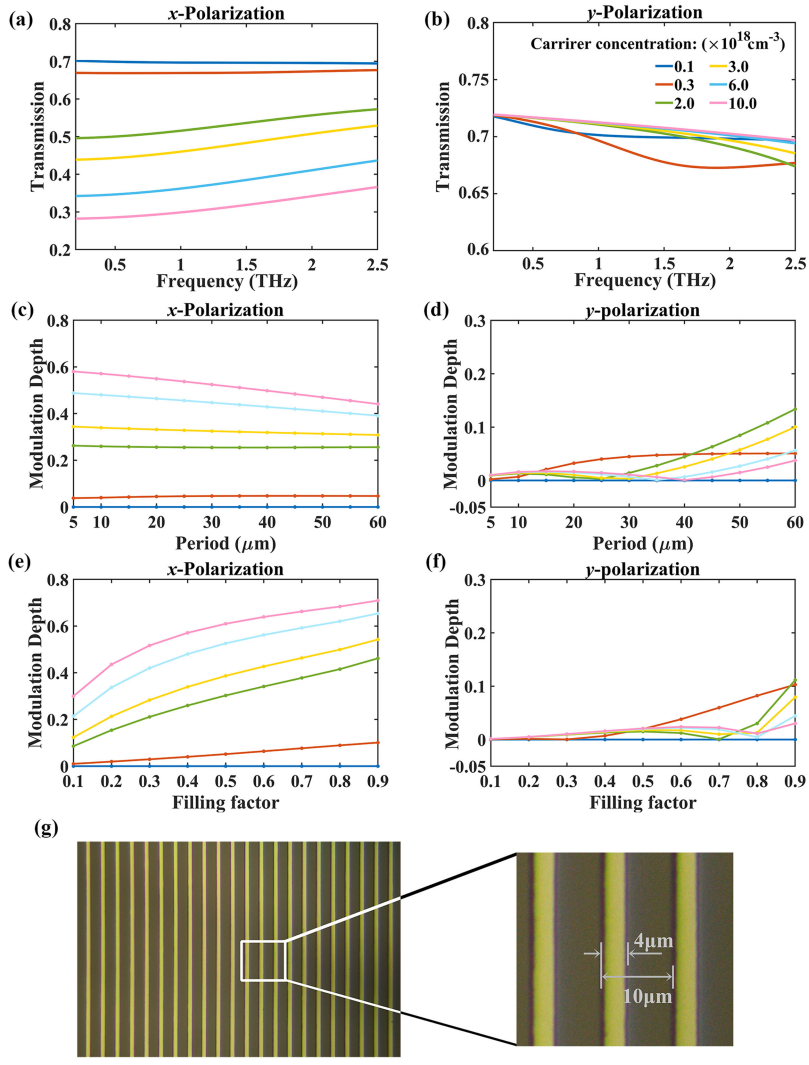

Fig. 2. Simulated THz transmission spectra of the SOS grating depending on the Si carrier concentration for (a) *x*-polarized and (b) *y*-polarized THz wave, with period and filling factor of grating set to 10 μm and 0.4. (c–d) The effect of period on the modulation of *x*-polarized and *y*-polarized THz wave at 1THz, with filling factor kept as 0.4. (e–f) The effect of filling factor on the modulation of *x*-polarized and *y*-polarized THz wave at 1THz, with a period of 10 μm. (g) Optical microscopy images of the fabricated SOS-grating metasurface. The width of Si (yellow part) is 4 μm and the period of grating is 10 μm.

3.2 Experimental Methods

We employed a home-built terahertz time-domain-spectroscopy (THz-TDS) and optical-pump-terahertz-probe (OPTP) system as shown in Fig. 3, to proceed our experimental study of our SOS metamaterial. Briefly, these optical systems are based on a Ti:sapphire regenerative amplifier (Spitfire-Ace, Spectra Physics). The output laser has 35 fs pulse width and its central wave-length is 800 nm with a repetition rate of 1 kHz. In our optical system, the output laser is split into three beams, separately used for THz generation, THz detection and optical pump of our metamaterials. Terahertz radiation was generated by optical rectification in a 0.5 mm-thick (110)-oriented ZnTe nonlinear crystal and was focused into THz beam by off-axis-parabolic (OAP) mirrors then through the sample. The THz beam electric field signal is measured by electro-optic sampling by letting the THz beam and THz detection beam through another 0.5 mm-thick (110)-oriented ZnTe crystal. The optical pump pulse was focused on the sample with a diameter of 7 mm at an incidence of

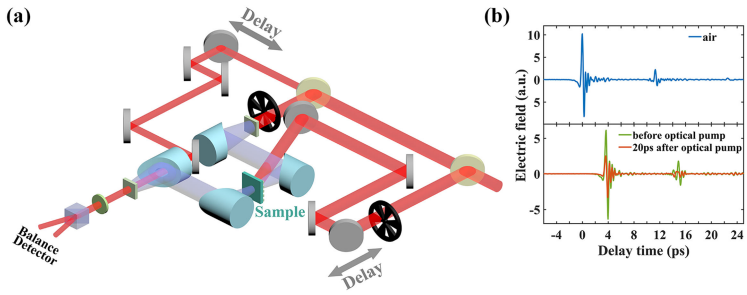

Fig. 3. (a) Schematic illustration of the home-built THz-TDS and OPTP system. The ultrafast femtosecond laser beam is split into three beams, respectively used for THz generation, THz detection and ultrafast optical pump. (b) Time-domain spectra of air, SOS-metasurface without optical pump and after optical pump. The THz pulse of air has a multi-reflection signal at t = 11.5 ps due to the multi-reflection effect of ZnTe.

about 20°. The time-domain THz pulse of air was measured and served as a reference, as shown in Fig. 3(b). The second pulse appeared at 11.3 ps in the THz signal of air results from Fabray–Perot (FP) reflections in ZnTe crystal (The refractive index of ZnTe is n = 3.1∼3.3 in THz range [27]). And the time-domain THz pulses of SOS-grating metasurface before/after optical pump are also demonstrated in Fig. 3(b). With a refractive index of Sapphire (n = 3.24), the signal caused by FP effect in Sapphire substrate is delayed by t = 2nh/c = 11.5 ps from the main signal. Therefore, the multi-reflecting terahertz wave of ZnTe and sapphire substrate have similar time delay in optical path, causing overlapping of these FP reflections in the second THz pulse when measuring the sample. In order to remove the FP reflections, the signal ranging from −5 ps to 11ps was chosen to calculate the Fourier transformation, without causing distortion in the main THz pulse. The frequency-domain transmission spectrum of metasurface is defined as $|\tilde{t}(\omega)| = |\tilde{E}_S(\omega)/\tilde{E}_R(\omega)|$, where $\tilde{E}_S(\omega)$ and $\tilde{E}_R(\omega)$ are Fourier transforms of the measured time-domain THz pulse of sample and the air reference, respectively.

In the OPTP measurement, the peak electric field of the time-domain THz pulse was measured by varying the time delay between the optical pump beam and the THz beam controlled by a linear motion controller. And the step length of motion controller is $\Delta d = 5\ \mu$m, thus the resolution of our time-domain data is $\Delta t = 2 * \Delta d/c = 33.4$ fs where c represents the light speed in vacuum. In addition, the measurement resolution of sample is also affected by the pulse width of pump beam and the experimental conditions, which will be discussed in Section 3.3.

3.3 Ultrafast Optical Modulation

The OPTP spectrum of four different types of *p*-doped SOS-grating metasurface for different polarization of THz wave are shown in Fig. 4. Transient variations of THz peak electric field in the time-domain signal for the *x*-polarized and *y*-polarized THz wave are presented in Figs. 4(a) and 4(b), from which it can be seen that the *x*-polarized THz wave is significantly modulated by the femtosecond pump laser pulse up to more than 60%, while the *y*-polarized THz beam is almost not modulated (less than 1%), agreeing well with the simulation results. From the subgraph in Fig. 4(a), it can be seen the modulation is rapidly switched on within 7 ps, and goes deeper until about 20 ps (except for the sample with 10^{15} cm^{-2} B^+ implantation and without RTA, because of its much short relaxation time). While in reality, the carriers in Si are generated within femtoseconds [28]. The switch speed of modulation is slowed down mainly by the following reasons. Firstly, the optical pump beam onto the sample has a pulse width about one hundred femtoseconds due to dispersion. Secondly, the pump beam is obliquely incident onto the metasurface at an angle of 20°, which leads to the nonsimultaneous excitation of the metasurface. Other effects such as carrier diffusion possibly contributes to the slow onset. The recombination time varies with the different type of *p*-doped Si. And the relaxation time of different type of SOS- grating was fitted by a mono-exponential function ($\Delta E/E_0 = A \cdot exp(-t/\tau_{relax})$) and shown as legend in Fig. 4(a).

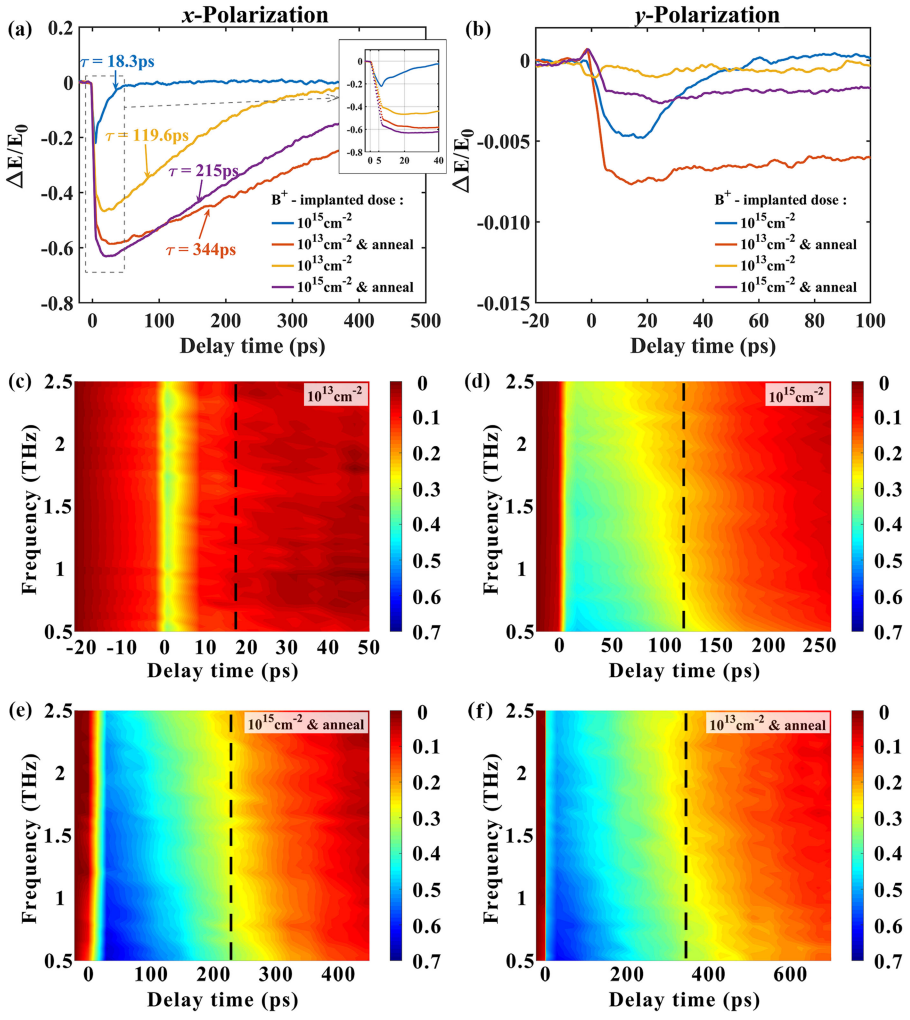

Fig. 4. Experimental OPTP spectrum at a pump power density of 1.3 mJ·cm^{-2} for four types of SOS-grating samples implanted by B^+ at dose of 10^{15} cm^{-2} or 10^{13} cm^{-2}, with/without RTA post-processing. Transient variation of THz peak electric field in the time-domain signal for the (a) *x*-polarized and (b) *y*-polarized THz wave. The relaxation time of different samples are labelled in (a) for the *x*-polarized wave. (c–f) Transient different modulation depth spectrum maps ($\Delta T(\omega)/T_0(\omega)$) for the four types of samples. The dash line represents the relaxation time of every sample calculated from Fig. 4(a), respectively.

As we can know, a higher implantation dose results in more crystal defects which heavily reduces the carrier lifetime of Si. Therefore, the SOS grating with implantation dose of 10^{15} cm^{-2} and without RTA presents a shorter relaxation time, but a lower modulation depth than that of 10^{13} cm^{-2} implanted and without RTA sample. RTA post-procession can repair the crystal defects caused by ion implantation and activate the implanted B^+, and thus improves the carrier density and extend the lifetime of photo-carriers. So it can be seen in Fig. 4(a) that RTA post-processed sample has a greatly higher modulation depth, but much longer relaxation time than those without RTA post-procession. Compared with the sample implanted with 10^{13} cm^{-2} and annealed, sample implanted with 10^{15} cm^{-2} and annealed exhibits a higher modulation depth and shorter relaxation time. It is because for the annealed samples, a higher implantation dose leads to more photo-generated carriers and thus a higher modulation depth. For the heavily doped Si, Auger recombination [29] occurs. So more photo-generated carriers will result in shorter carrier lifetime.

Figs. 4(c)–4(f) shows the photo-induced change in the transmittance of the THz spectrum for the four different type of SOS-grating metasurface as a function of pump pulse delay time at 1.3 mJ·cm^{-2}

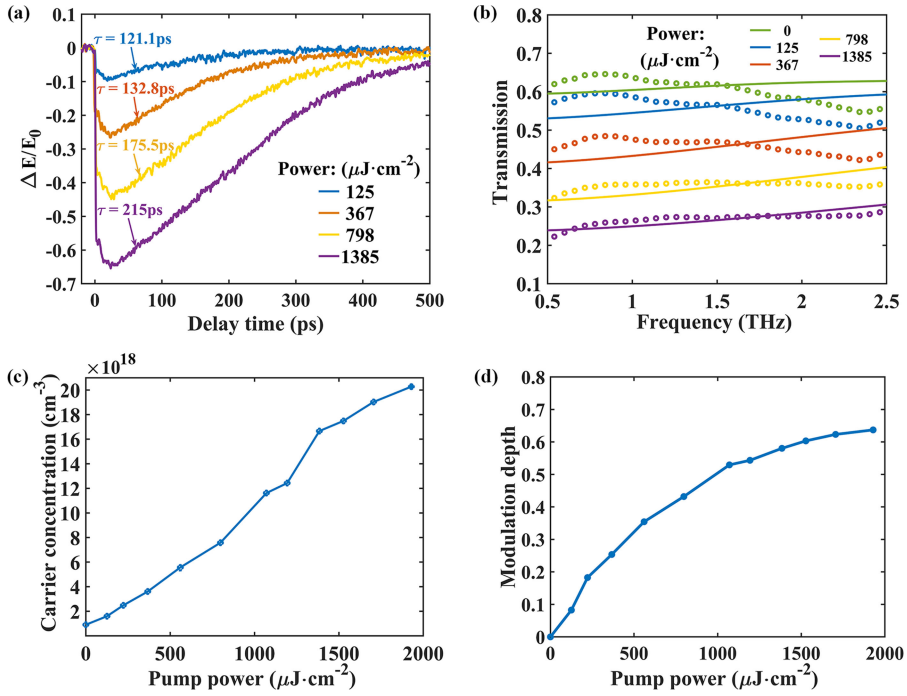

Fig. 5. Experimental results of 10^{15} cm^{-2} B^+ implanted and annealed sample with different optical pump power density. (a) Transient variation of THz peak electric field in the time-domain signal at different pump power. The relaxation time calculated by mono-exponential fitting is also shown. (b) THz transmission spectra with different pump power. The circle dots represent the experimental data and the solid lines represent the fitted results with theoretical model derived in section 3.5. (c) Fitted carrier concentration as a function of pump power density. (d) Modulation depth at 1 THz as a function of pump power density.

per pulse. Data in these color-map represents the variation of the electric field modulation depth as a function of optical pump delay time and terahertz wave frequency, which is calculated as $|\Delta T(\omega)/T_0(\omega)| = |T(\omega) - T_0(\omega)|/T_0(\omega)$. Each type of SOS-grating shows a broadband (0.5–2.5 THz) and ultra-fast modulation of the *x*-polarized THz wave. In short, the sample implanted with 10^{15} cm^{-2} B^+ presents the fastest broadband THz wave modulation with switch on-off time within 20 ps and a modulation depth of 20%, while the sample with 10^{15} cm^{-2} implanted and RTA shows the highest modulation depth about 60% (calculated at 1 THz) and a switch on-off time about 300 ps.

3.4 Experimental Results Under Different Pump Power Density

Furthermore, we studied the ultrafast modulation performance at different power density of pump pulse. The results are shown in Fig. 5. Fig. 5(a) shows that at different pump power the SOS-grating sample shares the similar modulation process. The optical-induced modulation all reaches to the maximum in 20 ps, but the relaxation time varies with the pump power density. As the pump power density increases, the grating sample shows a relatively long relaxation time. It can be inferred from Fig. 5(c) that a higher pump power density induces a higher concentration of photo-carriers, which requires a longer relaxation time for photo-carriers to recombine.

Fig. 5(b) demonstrates that the grating all achieves broad-band modulation at different pump power and a higher pump power density leads to a better modulation effect. Using the theoretical model derived in section 3.5, we can fit the experimental data in Fig. 5(b) and extract the carrier concentration shown in Fig. 5(c). We can infer from Figs. 5(c) and 5(d) that the carrier concentration almost linearly increases with increasing pump power density, but the modulation depth is almost saturated at a high pump power density over 1.3 mJ·cm^{-2}. As a result, the SOS-grating metasurface

with 10^{15} cm^{-2} ion implantation and RTA achieves the highest modulation depth which is relatively saturated at 1.3 mJ·cm^{-2} optical pump.

3.5 Numerical Fitting of Ultrafast Carriers' Dynamics

With the highest modulation depth and a relatively short relaxation time, the sample with 10^{15} cm^{-2} ion implantation and RTA was used to further investigate the ultrafast modulation process. The zeroth-order effective permittivity of the grating metastructure under different polarization can be calculated and described as [30]:

$$\varepsilon_{x\_pol} = n_{x\_pol}^2 = f\varepsilon_{Si} + (1-f)\varepsilon_{air} \tag{3}$$

$$\varepsilon_{y\_pol} = n_{y\_pol}^2 = \left(\frac{1-f}{\varepsilon_{air}} + \frac{f}{\varepsilon_{Si}}\right)^{-1} \tag{4}$$

In the equation, f represents the filling factor of the grating metastructure, and ε_{Si} and ε_{air} represents the dielectric coefficient of silicon and air. Additionally, ε_{Si} can be calculated by Drude model in Eqs. (1) and (2). According to Fresnel Equation, the transmission coefficient and reflection coefficient on the interface between two mediums (temporarily written as a and b) can be calculated as:

$$\tilde{t}_{a,b} = \frac{2\tilde{n}_a}{\tilde{n}_a + \tilde{n}_b} \tag{5}$$

$$\tilde{r}_{a,b} = \frac{\tilde{n}_a - \tilde{n}_b}{\tilde{n}_a + \tilde{n}_b} \tag{6}$$

Considering air space as media 1, the grating metastructure as media 2, and the sapphire substrate as media 3, whose effective refractive index are written as $\tilde{n}_1$, $\tilde{n}_2$ and $\tilde{n}_3$, respectively. As is described in Section 3.2, we chose the measurement window without the FP effect caused by sapphire substrate. The transmittance of SOS-grating can be described as [31]–[34]:

$$\tilde{t} = \tilde{t}_{1,2} * \widetilde{FP}_2 * \tilde{t}_{2,3} * \tilde{t}_{3,1} \tag{7}$$

While $\tilde{t}_{1,2}$, $\tilde{t}_{2,3}$ and $\tilde{t}_{3,1}$ represent the complex transmission coefficient of every interface in our model. The FP effect coefficient caused by the grating metastructure can be calculated as:

$$\widetilde{FP}_2 = \sum_{k=0}^{+\infty} \left\{ \tilde{r}_{2,1}\tilde{r}_{2,3} exp\left[-i\frac{2\tilde{n}_2\omega d}{c}\right]\right\}^k \tag{8}$$

where $\tilde{r}_{2,1}$ and $\tilde{r}_{2,3}$ are complex reflection coefficient of every interface in our model. Thus the transmittance of SOS-grating is a function of the SOS-metasurface effective dielectric constant and thus a function of ε_{Si}. By employing Eqs. (3), (5∼8), (1) and (2), we can derive an analytical relevance between the transmittance and the carrier parameters of Si:

$$\tilde{t} = \frac{2\tilde{n}_1}{\tilde{n}_1 + \tilde{n}_2} * \frac{1}{1 - \frac{(\tilde{n}_2 - \tilde{n}_1)(\tilde{n}_2 - \tilde{n}_3)}{(\tilde{n}_2 + \tilde{n}_1)(\tilde{n}_2 + \tilde{n}_3)} exp\left[-i\frac{2\tilde{n}_2\omega d}{c}\right]} * \frac{2\tilde{n}_2}{\tilde{n}_2 + \tilde{n}_3} * \frac{2\tilde{n}_3}{\tilde{n}_3 + \tilde{n}_1} \tag{9}$$

$$\tilde{n}_2 = \left[(1-f)\varepsilon_{air} + f\left(\varepsilon_\infty - \frac{Ne^2}{\varepsilon_0 m^*\left(\omega^2 + i\omega/\tau_d\right)}\right)\right]^{1/2} \tag{10}$$

Fig. 6(a) shows the experimental transmission spectra (circle dots) of SOS-grating with 10^{15} cm^{-2} B^+ implanted and RTA at several pump-probe delay values. And then we fitted the experimental spectra employing Eq. (9) to obtain the transient Si carrier concentration, with theoretically fitted spectra shown in Fig. 6(a) (solid lines) and the extracted carrier concentration presented in Fig. 6(b), respectively. As can be seen, there are some small differences between the fitted results and

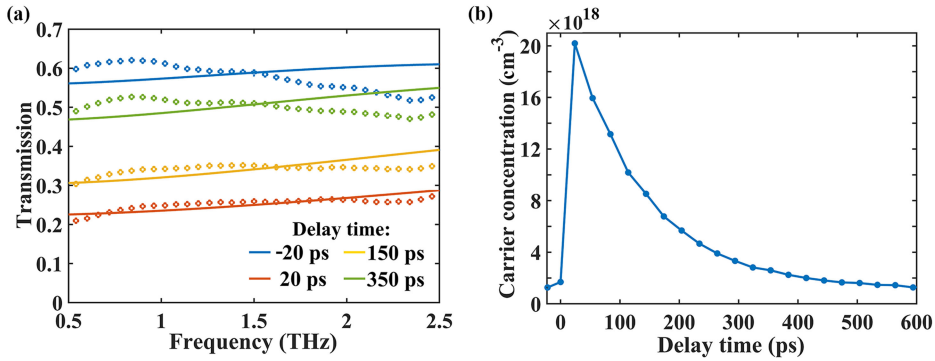

Fig. 6. Experimental and numerical fitting results of SOS-grating with 10^{15} cm^{-2} B^+ implanted and RTA post-processed. (a) THz transmission spectra at different pump-probe delays. The circle dots represent the experimental data and the solid lines represent the fitted results. (b) Numerical fit of Si carrier concentration as a function of pump-probe delay time.

measurement ones. In the numerical fitting of experimental data, to simply the fitting process, only the carrier concentration was set as free parameter, with the effective mass of the carriers $m*$ and the carrier scattering rate τ_d is kept unchanged. However, values of $m*$ and τ_d may also have little change in the optical pumping, so simplification in our fitting may result in this little misalign. In Fig. 6(b), it's shown the carrier concentration multiplies about 10 times at optical pump excitation and as the photo-carriers recombine, the carrier concentration reduces to the unexcited level.

Therefore, the transmission spectra in Fig. 6(a) can be clearly explained. At −20 ps, no pump pulse is interacted with Si, thus the carriers in Si remain unexcited. At 0 ps, pump pulse firstly excites the photo-carriers in Si which can be seen from the spectra that the transmittance has a drastic reduction. 20 ps later, the modulation depth reaches its maximum and the photo-carriers recombines as the delay time proceeds. At around 300 ps, the photo-excited carriers almost recombine to the unexcited state, and thus the transmission spectrum returns to the initial state. On the other hand, from Fig. 6(b), the extracted maximum value of photo-carrier concentration is on the order of 10^{19} cm^{-3}. With such carrier concentration value, the simulated modulation depth is about 60% estimated from Fig. 2, which agrees well with the experimental results.

4. Conclusion

In summary, we have theoretically and experimentally demonstrated the ultrafast, broadband and polarization-selective THz modulator based on the grating-like metasurface on heavily *p*-doped Silicon-On-Sapphire film. We have fabricated four types of SOS gratings to investigate the effect of ion implantation and annealing on the performance of modulator. And the experimental results presented that the sample with 10^{15} cm^{-2} B^+ implanted and annealed showed the highest modulation depth about 60% for the *x*-polarized THz wave at 1 THz and less than 1% for the *y*-polarized THz wave in the frequency ranging from 0.5 to 2.5 THz, with a switch on-off time about 300 ps. The experimental results also showed the modulation depth increased with the increasing pump power density, but was almost saturated at a pump power density over 1.3 mJ·cm^{-2}. Moreover, the relationship between dynamics of photo-generated carriers' concentration and the ultrafast modulation effects has been well investigated. And it can be concluded that the ultrafast excitation and recombination of photo-carriers in Si is attributed to the ultrafast modulation of THz wave. Our results may pave a way to achieve ultrafast THz optics.

Acknowledgment

The device fabrication in this work was partially carried out at the USTC Center for Micro and Nanoscale Research and Fabrication.

References

[1] C. M. Watts *et al.*, "Terahertz compressive imaging with metamaterial spatial light modulators," *Nature Photon.*, vol. 8, pp. 605–609, 2014.
[2] R. Fukasawa, "Terahertz imaging: Widespread industrial application in non-destructive inspection and chemical analysis," *IEEE Trans. THz Sci. Technol.*, vol. 5, no. 6, pp. 1121–1127, Nov. 2015.
[3] T. Nagatsuma, G. Ducournau, and C. C. Renaud, "Advances in terahertz communications accelerated by photonics," *Nature Photon.*, vol. 10, pp. 371–379, 2016.
[4] H. T. Stinson *et al.*, "Imaging the nanoscale phase separation in vanadium dioxide thin films at terahertz frequencies," *Nature Commun.*, vol. 9, 2018, Art. no. 3604.
[5] Q. Mao *et al.*, "High-speed and broadband terahertz wave modulators based on large-area graphene field-effect transistors," *Opt. Lett.*, vol. 39, pp. 5649–5652, 2014.
[6] T. Wen *et al.*, "Semiconductor terahertz modulator arrays: The size and edge effect," *Opt. Lett.*, vol. 43, pp. 3021–3024, 2018.
[7] H. Cai *et al.*, "Multifunctional hybrid metasurfaces for dynamic tuning of terahertz waves," *Adv. Opt. Mater.*, vol. 6, 2018, Art. no. 1800257.
[8] H. K. Yoo *et al.*, "Highly efficient terahertz wave modulators by photo-excitation of organics/silicon bilayers," *Appl. Phys. Lett.*, vol. 105, 2014, Art. no. 011115.
[9] P. Weis, J. L. Garcia-Pomar, M. Höh, B. Reinhard, A. Brodyanski, and M. Rahm, "Spectrally wide-band terahertz wave modulator based on optically tuned graphene," *ACS Nano*, vol. 6, pp. 9118–9124, 2012.
[10] Q.-Y. Wen *et al.*, "Graphene based all-optical spatial terahertz modulator," *Sci. Rep.*, vol. 4, 2015, Art. no. 7409.
[11] Q. Li *et al.*, "Active graphene–silicon hybrid diode for terahertz waves," *Nature Commun.*, vol. 6, 2015, Art. no. 7082.
[12] G. Zhou *et al.*, "Broadband and high modulation-depth THz modulator using low bias controlled VO_2-integrated metasurface," *Opt. Exp.*, vol. 25, pp. 17322–17328, 2017.
[13] X. Liu *et al.*, "Terahertz broadband modulation in a biased $BiFeO_3$/Si heterojunction," *Opt. Exp.*, vol. 24, pp. 26618–26628, 2016.
[14] A. Chanana, X. Liu, C. Zhang, Z. V. Vardeny, and A. Nahata, "Ultrafast frequency-agile terahertz devices using methylammonium lead halide perovskites," *Sci. Adv.*, vol. 8, 2018, Art. no. eaar7353.
[15] H.-T. Chen *et al.*, "Ultrafast optical switching of terahertz metamaterials fabricated on ErAs/GaAs nanoisland superlattices," *Opt. Lett.*, vol. 32, pp. 1620–1622, 2007.
[16] S. J. M. Rao, G. Kumar, A. K. Azad, and D. R. Chowdhury, "Ultrafast relaxation of charge carriers induced switching in terahertz metamaterials," *J. Infrared, Millimeter, Terahertz Waves*, vol. 39, pp. 1211–1220, 2018.
[17] L. Fekete, F. Kadlec, P. Kužel, and H. Němec, "Ultrafast opto-terahertz photonic crystal modulator," *Opt. Lett.*, vol. 32, pp. 680–682, 2007.
[18] W. X. Lim *et al.*, "Ultrafast all-optical switching of germanium-based flexible metaphotonic devices," *Adv. Mater.*, vol. 30, 2018, Art. no. 1705331.
[19] Y. K. Srivastava *et al.*, "MoS_2 for ultrafast all-optical switching and modulation of THz Fano metaphotonic devices," *Adv. Opt. Mater.*, vol. 5, 2017, Art. no. 1700762.
[20] H. Cai *et al.*, "All-optical and ultrafast tuning of terahertz plasmonic metasurfaces," *Adv. Opt. Mater.*, vol. 6, 2018, Art. no. 1800143.
[21] Y. Yang *et al.*, "Transient GaAs plasmonic metasurfaces at terahertz frequencies," *ACS Photon.*, vol. 4, pp. 15–21, 2017.
[22] K. P. H. Lui and F. A. Hegmann, "Fluence- and temperature-dependent studies of carrier dynamics in radiation-damaged silicon-on-sapphire and amorphous silicon," *J. Appl. Phys.*, vol. 93, pp. 9012–9018, 2003.
[23] N. Shen *et al.*, "Optically implemented broadband blueshift switch in the terahertz regime," *Phys. Rev. Lett.*, vol. 106, 2011, Art. no. 037403.
[24] S. Nashima, O. Morikawa, K. Takata, and M. Hangyo, "Measurement of optical properties of highly doped silicon by terahertz time domain reflection spectroscopy," *Appl. Phys. Lett.*, vol. 79, pp. 3923–3925, 2001.
[25] K. Sokolowski-Tinten and D. von der Linde, "Generation of dense electron-hole plasmas in silicon," *Phys. Rev. B*, vol. 61, pp. 2643–2650, 2000.
[26] K. Cho, M. Numan, T. G. Finstad, W. K. Chu, J. Liu, and J. J. Wortman, "Transient enhanced diffusion during rapid thermal annealing of boron implanted silicon," *Appl. Phys. Lett.*, vol. 47, pp. 1321–1323, 1985.
[27] A. Nahata, A. S. Weling, and T. F. Heinz, "A wideband coherent terahertz spectroscopy system using optical rectification and electro-optic sampling," *Appl. Phys. Lett.*, vol. 69, pp. 2321–2323, 1996.
[28] T. Sjodin, H. Petek, and H.-L. Dai, "Ultrafast carrier dynamics in silicon: A two-color transient reflection grating study on a (111) surface," *Phys. Rev. Lett.*, vol. 81, pp. 5664–5667, 1998.
[29] Z. Yuan *et al.*, "Silicon nanocrystals as an enabling material for silicon photonics," *Proc. IEEE*, vol. 97, no. 7, pp. 1250–1268, Jul. 2009.
[30] L. Cong, N. Xu, J. Han, W. Zhang, and R. Singh, "A tunable dispersion-free terahertz metadevice with Pancharatnam-Berry-phase-enabled modulation and polarization control," *Adv. Mater.*, vol. 27, pp. 6630–6636, 2015.
[31] L. Duvillaret, F. Garet, and J.-L. Coutaz, "A reliable method for extraction of material parameters in terahertz time-domain spectroscopy," *IEEE J. Sel. Topics Quantum Electron.*, vol. 2, no. 3, pp. 739–746, Sep. 1996.
[32] N. K. Grady *et al.*, "Terahertz metamaterials for linear polarization conversion and anomalous refraction," *Science*, vol. 340, pp. 1304–1307, 2013.
[33] X. Zhao *et al.*, "Optically modulated ultra-broadband all-silicon metamaterial terahertz absorbers," *ACS Photon.*, vol. 6, pp. 830–837, 2019.
[34] X. Zhao *et al.*, "Nonlinear terahertz metamaterial perfect absorbers using GaAs [Invited]," *Photon. Res.*, vol. 4, pp. A16–A21, 2016.